

# Synthesis and characterization of photo- and pH-responsive nanoparticles containing amino-substituted azobenzene†

Qian Tang,<sup>a</sup> Xianzhu Meng,<sup>a</sup> Hongbo Jiang,<sup>a</sup> Tianyou Zhou,<sup>a</sup> Chengbin Gong,<sup>\*a</sup> Xiangkai Fu<sup>a</sup> and Sanqiang Shi<sup>b</sup>

Received 28th April 2010, Accepted 10th July 2010

DOI: 10.1039/c0jm01235a

A novel dual responsive nanomaterial sensitive to both photo- and pH stimuli has been successfully developed. The polymer-based nanoparticles were fabricated from a specially designed photo- and pH-responsive amino-substituted azobenzene monomer, 4-amino-4'-methacrylatylazobenzene (AMAAB), *via* free radical polymerization with trimethylolpropane trimethacrylate (TRIM) cross-linkers. The *trans-cis* photoisomerization properties of AMAAB were retained after incorporation into the rigid three-dimensional cross-linked polymer matrix. The TRIM/AMAAB molar ratio significantly influenced the kinetics of the *trans-cis* photoisomerization. The nanoparticles also possessed good pH-responsive properties. The change in absorbance with media pH was monitored at 402 nm, and a "titration type" curve was obtained with a  $pK_a$  value of  $0.61 \pm 0.06$ . At this transition point, the color of the nanoparticle suspension changed colour from yellow to pink. Thermogravimetric analysis (TGA) indicated that the nanoparticles were thermally stable.

## 1. Introduction

Stimuli-responsive materials, also known as smart materials, have aroused increasing interest in material science and technology for their good performance in energy transfer,<sup>1</sup> drug delivery,<sup>2</sup> data storage<sup>3,4</sup> and biotechnology.<sup>5</sup> Azobenzene-containing polymers are a very popular class of photo-responsive materials because of their wide scope of applications in nonlinear optics,<sup>6-9</sup> optical storage,<sup>10,11</sup> holography<sup>12</sup> and liquid crystal displays.<sup>13</sup> Most of these applications utilized photo-responsive materials that contained azobenzenes either as backbones or as side-chains of linear polymers. On the other hand, reports on materials with azobenzenes embedded into three-dimensional network of polymers are scarce. Recently, multi-functional materials<sup>14</sup> have also come into being, supporting applications in more extended domains. These multi-functional materials are constructed from various smart elements that can respond to different stimuli, such as light,<sup>1</sup> temperature,<sup>15,16</sup> pH<sup>17</sup> and even specific molecular species,<sup>18</sup> in a co-operative manner.

At one stage, it was generally believed that amino-substituted azobenzenes were not suitable for photo-responsive materials because of the strong electron-donating effect of the amino group that tended to induce the overlapping of the  $\pi-\pi^*$  and  $n-\pi^*$  transitions of the chromophores. As a result, the weak  $n-\pi^*$  band could be masked by the  $\pi-\pi^*$  absorption, resulting in the irreversible photoisomerization of aminoazobenzenes.<sup>19</sup> For this reason, studies on the photoisomerization of aminoazobenzenes

were much fewer than the other non-amino substituted azobenzene compounds.<sup>20-26</sup>

In this paper, through a delicate molecular design, a tri-functional amino-substituted azobenzene, 4-amino-4'-methacrylatylazobenzene (AMAAB), was successfully synthesized and studied for its spectroscopic responses towards selected external stimuli. It was observed that AMAAB underwent reversible photoisomerization in the UV/vis spectral range which has rarely been reported before. Besides its photo-response, the amino functionality of AMAAB also brought about its pH-responsive properties. Using AMAAB as the monomer, TRIM as the cross-linker, and AIBN as the radical initiator, a novel dual photo- and pH-responsive nanomaterial was fabricated. The morphology and thermal properties, as well as the photo- and pH-response of the nanoparticles were characterized *via* atomic force microscopy (AFM), thermogravimetric analysis (TGA) and UV/vis spectroscopy.

## 2. Experimental

### 2.1 Materials and apparatus

Methacryloyl chloride was prepared from methacrylic acid with thionyl chloride. All the other reagents were commercially supplied and purified by the usual methods. <sup>1</sup>H NMR and <sup>13</sup>CNMR (300MHz) were performed on a Bruker AV-300 NMR instrument at ambient temperature, with TMS as the internal standard. Elemental analysis was performed by a Leco CHN-900 micro carbon-hydrogen-nitrogen analyzer. Gas chromatography mass spectrometry (GC-MS) chromatograms were obtained using an Agilent 6890 GC system coupled to an Agilent 5973 quadrupole mass selective detector. UV/cis spectra were recorded with an UV-4802 spectrophotometer (UNICO(Shanghai)Instruments Co., Ltd.). A GY-13 50W high pressure Hg lamp (Tianjin Tuopu Instrument Co., Ltd.) coupled with a DS-3 monochromator (Tianjin Tuopu Instrument Co., Ltd.; slit: 4 mm) was used as the light

<sup>a</sup>College of Chemistry and Chemical Engineering, Southwest University, Beibei, Chongqing, China 400715. E-mail: gongcbtq@swu.edu.cn; Fax: +86-23-68254000; Tel: +86-23-68252360

<sup>b</sup>Department of Mechanical Engineering, The Hong Kong Polytechnic University, Hong Kong, China

† Electronic supplementary information (ESI) available: NMR spectra, UV/vis spectra and photograph of the AMAAB solution. See DOI: 10.1039/c0jm01235a

source in the photoisomerization studies. pH measurement was performed with a PHS-3D pH meter (Shanghai Precision & Scientific Instrument Co., Ltd.). The morphology of the nanoparticles was determined by a DI Multimode SPM (Veeco Instruments Inc., USA) operated in tapping mode with a TESPT cantilever. Spin-coating was carried out by spin coater SC-1B (Beijing Chuangshiweina Instrument Co., Ltd.). The thermal stability of the samples was determined by thermogravimetric analysis (TGA) using a SDT Q600 thermal analyzer (USA) at a heating rate of 10 °C min<sup>-1</sup> up to 700 °C under flowing N<sub>2</sub> (100 mL min<sup>-1</sup>). Melting points were measured on a X-6 melting point apparatus (Beijing Fukai Instrument Co., Ltd.).

## 2.2 Synthesis of 4-Nitro-4'-hydroxylazobenzene (NHOAB)

4-nitroaniline (2.76 g, 0.020 mol) was dissolved in a solution of concentrated sulfuric acid (4.4 mL) and distilled water (10 mL) by gently heating and stirring. Then the solution was cooled with ice water and the temperature was kept below 1 °C. A cooled solution (12 mL) of NaNO<sub>2</sub> (1.52 g, 0.022 mol) was then added dropwise. The resultant diazonium salt solution was stirred for a further 15 min at 0–1 °C. An ice cold mixture of phenol (1.88 g, 0.020 mol) and distilled water (15 mL) was then poured into the diazonium salt solution, followed by neutralization (pH = 8–10) with cooled NaOH solution (10%). The mixture was stirred for about 2 h at 0–3 °C and then was acidified with a few drops of concentrated HCl. The crude product was obtained by filtration and purified by recrystallization in ethanol–H<sub>2</sub>O (v/v = 5 : 1) to produce 4.16 g of red crystal. Yield: 85.6%, <sup>1</sup>H NMR (δ, CDCl<sub>3</sub>): 5.42 (s, 1H), 7.10 (m, 2H), 8.06 (d, 4H), 8.50 (d, 2H), <sup>13</sup>CNMR (δ, CDCl<sub>3</sub>): 159.49, 156.13, 147.23, 125.98, 125.52, 124.81, 123.17, 116.22, GC-MS *m/z*: 243.1. Elemental analysis calculated (%) for C<sub>12</sub>H<sub>9</sub>N<sub>3</sub>O<sub>3</sub>: C 59.26, H 3.73, N 17.28, found: C 58.976, H 3.722; N 17.665.

## 2.3 Synthesis of 4-Nitro-4'-methacrylatylazobenzene (NMAAB)

A mixture of NHOAB (1.22 g, 0.005 mol), dichloromethane (30 mL) and triethylamine (acid scavenger, 1.05 mL, 0.0075 mol) was purged with nitrogen for 30 min and was then maintained in an ice bath. A solution of methacryloyl chloride (0.53 mL, 0.0055 mol) and dichloromethane (10 mL) was then added dropwise from a dropping funnel and triethylammonium salt in the form of smog was observed immediately. The resultant mixture was heated to 40 °C (reflux) for 4 h and the reaction was monitored by thin layer chromatography (TLC). Afterward, the mixture was washed thoroughly with distilled water to remove the triethylammonium salt. The organic layer was dried by anhydrous Na<sub>2</sub>SO<sub>4</sub>, and evaporated by rotary evaporation. The crude product was purified by recrystallization in ethyl acetate to produce 1.40 g of an orange powder. Yield: 89.7%. Mp: 126.7–128.0 °C. <sup>1</sup>H NMR (δ, DMSO-*d*<sub>6</sub>): 2.09 (s, 3H), 5.92 (s, 1H), 6.38 (s, 1H), 7.46 (m, 2H), 8.16 (d, 4H), 8.44 (d, 2H). <sup>13</sup>CNMR (δ, DMSO-*d*<sub>6</sub>): 165.43, 155.44, 154.21, 150.13, 149.11, 135.64, 128.92, 125.86, 125.02, 124.43, 123.61, 18.56 GC-MS *m/z*: 311. Elemental analysis calculated (%) for C<sub>16</sub>H<sub>13</sub>N<sub>3</sub>O<sub>4</sub>: C 61.73, H 4.21, N 13.50, found: C 61.835, H 4.441; N 13.615.

## 2.4 Synthesis of 4-Amino-4'-methacrylatylazobenzene (AMAAB)

Acetone (60 mL), distilled water (15 mL), NMAAB (1.55 g, 0.005 mol), zinc powder (2.6 g, 0.04 mol) and AlCl<sub>3</sub>•6H<sub>2</sub>O (0.4 g) were placed in a 250 mL three-necked flask which was fitted with a reflux condenser. The mixture was stirred at room temperature for 1 h, then warmed to 40 °C for 1 h, 50 °C for 3 h, and finally the mixture was refluxed at 60 °C for 2 h. TLC was utilized to monitor the reaction process. The resultant mixture was cooled to room temperature and suction filtered to remove the excess zinc powder, followed by evaporation under reduced pressure to give the crude product in the form of a golden precipitate. The product was obtained by filtration and recrystallization in ethanol to produce 0.82 g of yellow powder. Yield: 58.5%. Mp: 178.5–180.1 °C. <sup>1</sup>H NMR (δ, CDCl<sub>3</sub>): 2.08 (s, 3H), 4.06 (s, broad; 2H), 5.78 (s, 1H), 6.38 (s, 1H), 6.72 (d, 2H), 7.23 (d, 2H), 7.78 (m, 4H). <sup>13</sup>CNMR (δ, CDCl<sub>3</sub>): 165.65, 152.02, 150.57, 149.62, 145.51, 135.82, 127.54, 125.16, 123.45, 122.10, 114.65, 18.42 GC-MS *m/z*: 281. Elemental analysis calculated (%) for C<sub>16</sub>H<sub>15</sub>N<sub>3</sub>O<sub>2</sub>: C 68.31, H 5.37, N 14.94, found: C 68.19, H 5.339; N 14.99.

## 2.5 General preparation of nanoparticles

The nanoparticles were fabricated *via* free radical polymerization of AMAAB and TRIM in the presence of AIBN as a radical initiator. A series of nanoparticles with TRIM/AMAAB molar ratios of 50 : 1, 20 : 1, 10 : 1, 5 : 1, 3 : 1, and 1 : 1 were prepared. A typical procedure for the fabrication of NpT5A1 (a nanoparticle with a TRIM:AMAAB = 5 : 1) was as follows: a solution containing AMAAB (0.14 g, 0.0005 mol), TRIM (0.84 g, 0.0025 mol), AIBN (0.08 g), DMF (1.0 mL) and acetonitrile (50 mL) were deoxygenated with nitrogen for 30 min, the resulting solution was placed in an oil bath at 70 °C for 12 h in the dark to minimize isomerization of the azobenzene residues. The precipitate was obtained by centrifugation and washed several times with hot methanol. Finally, the product was dried under vacuum to constant weight and afforded a yellow powder.

## 2.6 Spectroscopic characterization and photoisomerization studies

Spectroscopic characterization of the functionalized azobenzene monomer and the subsequent nanoparticles were performed in DMF. Air-tight screw-capped quartz cells of 1.0 cm optical path length were used in all experiments. The suspension of nanoparticle material in the solvent media was maintained with the help of a magnetic stirrer. For the *trans* to *cis* photoisomerization studies, solutions or suspensions were stirred and irradiated at 405 nm (monochromator slit width: 4 mm), UV/vis spectra of the suspension were measured at regular time intervals. Stirring and irradiation was suspended during spectroscopic measurement. For the *cis* to *trans* photoisomerization studies, irradiation at 456 nm was adopted.

## 2.7 Atomic force microscopy

Thin films of nanoparticles on mica for AFM characterization were prepared by spin-coating (at 4000 rpm) of nanoparticle suspensions at a loading of 2.0 mg in 5 mL of ethanol. The suspensions were sonicated for 20 min before spin-coating.

## 2.8 Studies on pH responses

0.0042 g of NpT5A1 was suspended in 6.0 mL ethanol, followed by ultrasonic stirring for 20 min. Then, 500  $\mu$ L of the suspension was diluted into 5.0 mL with ethanol and distilled water ( $v/v = 1 : 1$ ). pH of the media was adjusted by the addition of HCl. Accurate pH of the media was measured by pH meter. UV/vis spectra were obtained 5 min after each pH adjustment.

## 3. Results and discussion

### 3.1 Preparation of monomer and nanoparticle

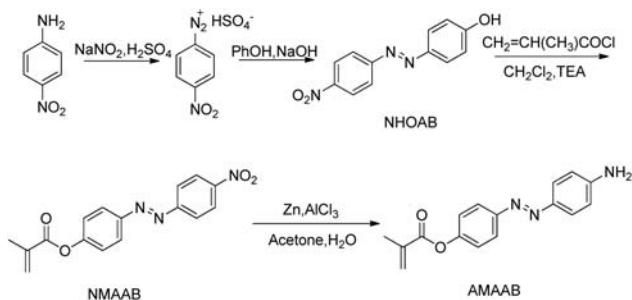
The synthesis of AMAAB was tedious due to the fact that it contains three different functional moieties in its molecular structure. Using *p*-nitroaniline as the starting material, AMAAB was synthesized *via* diazotization coupling, esterification and nitro reduction reactions. The yield of nitro reduction reaction was 58.5%, which was much higher than previously reported<sup>26</sup> (only 15% with the reduction reaction). The synthesis route is summarized in Scheme 1.

AMAAB is not easily soluble in acetonitrile, chloroform, methanol or THF, but soluble in DMF and DMSO. Thus, a mixture of acetonitrile and DMF was employed in the subsequent polymerization process. Without acetonitrile, the polymer particles obtained were too big to suspend in solvents. They had to be crushed, milled and wet sieved before UV/vis characterization, and the resultant particles had an irregular morphology. In the presence of acetonitrile as the porogen, regular AMAAB-based nanoparticles were formed. TRIM and other crosslinkers have been attempted. Nevertheless, nanoparticle materials fabricated from TRIM were found to show the best properties. In addition, different monomer : cross-linker mole ratios have been explored. The preparation process of the nanoparticles is shown in Scheme 2.

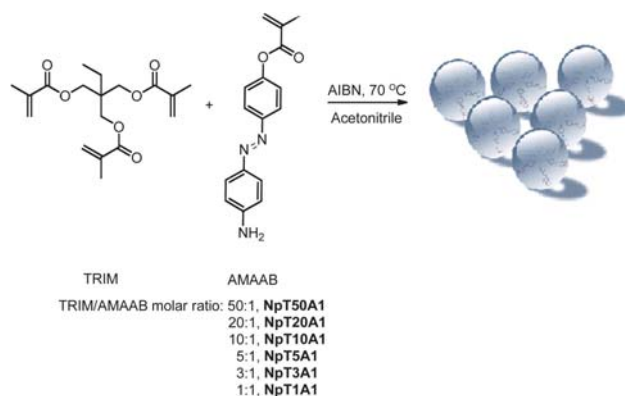
### 3.2 Photoresponsive properties

AMAAB was dissolved in DMF and the nanoparticles were suspended in DMF for the UV/vis measurements. Before the measurement, the sample solutions were kept in the dark at room temperature overnight to ensure that all of the azobenzene units were in the *trans* configuration.

Fig. 1a shows the UV/vis spectra and spectral changes of the AMAAB monomer in DMF solution ( $1.0 \times 10^{-5} \text{ mol L}^{-1}$ ) upon irradiation at 405 nm. Before irradiation, the maximum



**Scheme 1** The synthetic route for *trans*-4-amino-4'-methacrylatylazobenzene (AMAAB).



**Scheme 2** The preparation of nanoparticles with different TRIM/AMAAB molar ratios.

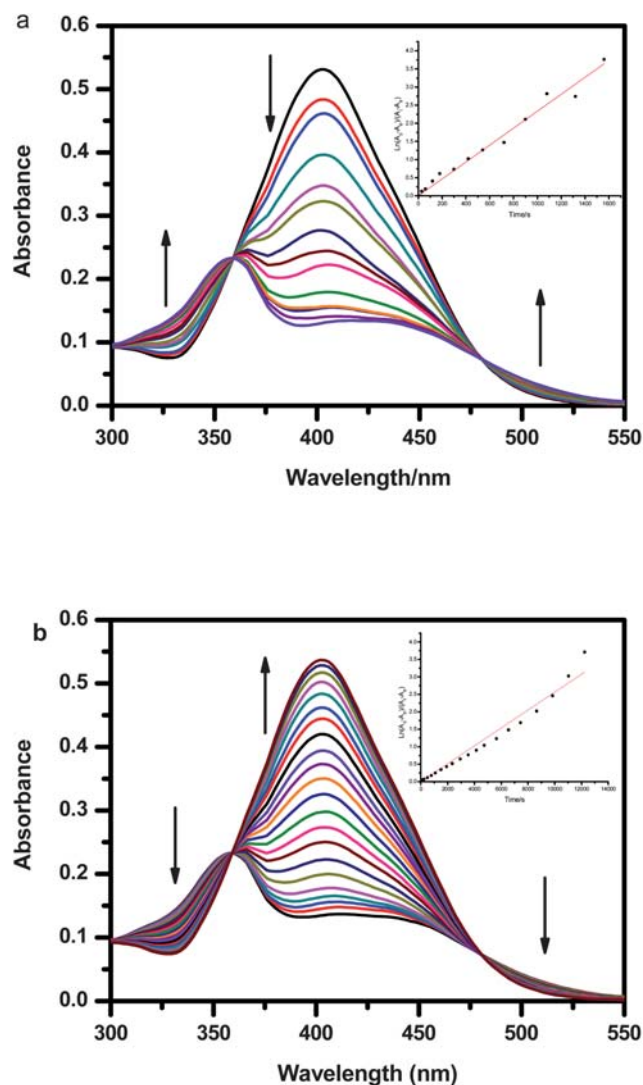


**Fig. 1** UV/vis spectra and spectral changes of AMAAB solution ( $1.0 \times 10^{-5} \text{ mol L}^{-1}$ , DMF) upon irradiation with 405 nm light for 0.5, 1, 2, 3, 5, 7, 9, 12, 15, 18, 22, 26, 30 min (a) and then upon irradiation with 456 nm light for 1, 2, 4, 8, 13, 18, 25, 32, 39, 49, 59, 69, 79, 94, 109, 124, 144, 164, 184, 204, 224 min (b). Insets: the kinetics of the photoisomerization of AMAAB.

absorption was observed at 402 nm, which was attributed to the  $\pi$ - $\pi^*$  transition of the azobenzene chromophore in its *trans* configuration. UV/Vis irradiation at 405 nm induced *trans*  $\rightarrow$  *cis* photoisomerization, resulting in a decrease in the absorbance at 402 nm, with twin isosbestic points at 360 and 482 nm.

After irradiation at 405 nm for 30 min, spectral changes of the AMAAB solution levelled off, indicating that the system reached a photostationary state. The original absorption peak at 402 nm disappeared and a new medium-strength peak was observed at 360 nm, which was attributed to the  $\pi$ - $\pi^*$  transition of the azobenzene chromophore in its *cis* configuration. Subsequent irradiation of the solution at 456 nm reversed the spectral change of the solution back to its original state within 224 min (Fig. 1b). This indicates that the photoinduced isomerization processes are fully reversible. Furthermore, it is worth mentioning that the absorption peak of the  $n$ - $\pi^*$  transition of the azobenzene chromophore of AMAAB was not observed because it was very weak and was masked by the strong and broad  $\pi$ - $\pi^*$  transition. Kinetics of the photoisomerization processes were analyzed by the first-order kinetics expression in eqn (1):

$$\ln \frac{(A_0 - A_\infty)}{(A_t - A_\infty)} = kt \quad (1)$$

where  $A_0$ ,  $A_t$  and  $A_\infty$  are the absorbances at 402 nm of the azobenzene chromophore at time 0,  $t$  and the photostationary state, respectively.

Rate constants for the *trans*  $\rightarrow$  *cis* and *cis*  $\rightarrow$  *trans* isomerization of AMAAB were found to be  $23.3 \times 10^{-4}$  and  $2.6 \times 10^{-4} \text{ s}^{-1}$ , respectively. It is interesting to notice that the *trans*  $\rightarrow$  *cis* rate was almost 10 times faster than the *cis*  $\rightarrow$  *trans* rate. This result might be also attributed to the superimposition of the  $\pi$ - $\pi^*$  transition on the  $n$ - $\pi^*$  transition. Irradiation at 456 nm excites both the  $n$ - $\pi^*$  and, to a lesser extent,  $\pi$ - $\pi^*$  transitions of the azobenzene chromophore simultaneously. This slows down the overall *cis*  $\rightarrow$  *trans* conversion.

Fig. 2 shows the spectroscopic responses of the AMAAB-based nanoparticles NpT5A1, toward irradiation at 405 nm and then 456 nm. Responses of the nanomaterial to photo-excitation were quite similar to that of the AMAAB monomer. This indicates that the azobenzene chromophore of the monomer has retained their photo-switching properties after being incorporated into the rigid three dimensional cross-linked polymer matrix. The extent of the spectral change of NpT5A1 was smaller than that of AMAAB, probably due to steric hindrance within the nanomaterial. Rate constants of the *trans*  $\rightarrow$  *cis* and *cis*  $\rightarrow$  *trans* isomerization of NpT5A1 were found to be  $(14.4 \pm 0.5) \times 10^{-4}$  and  $(7.4 \pm 0.3) \times 10^{-4} \text{ s}^{-1}$ , respectively. Other nanoparticles, NpT50A1, NpT20A1, NpT10A1, NpT3A1, and NpT1A1 exhibited similar photo-responsive behavior (see ESI†).

Nonetheless, significant differences in the photoisomerization properties of the AMAAB-based nanoparticles were observed. Firstly, the extent of spectral change upon irradiation was affected by the content of AMAAB in the nanoparticles. Both high proportion (as in NpT1A1 and NpT3A1) and low proportion (as in NpT50A1 and NpT20A1) of AMAAB diminished the extent of spectral change upon irradiation. The former was probably caused by the steric hindrance between adjacent azobenzene chromophores, resulting in incomplete photoisomerization. The

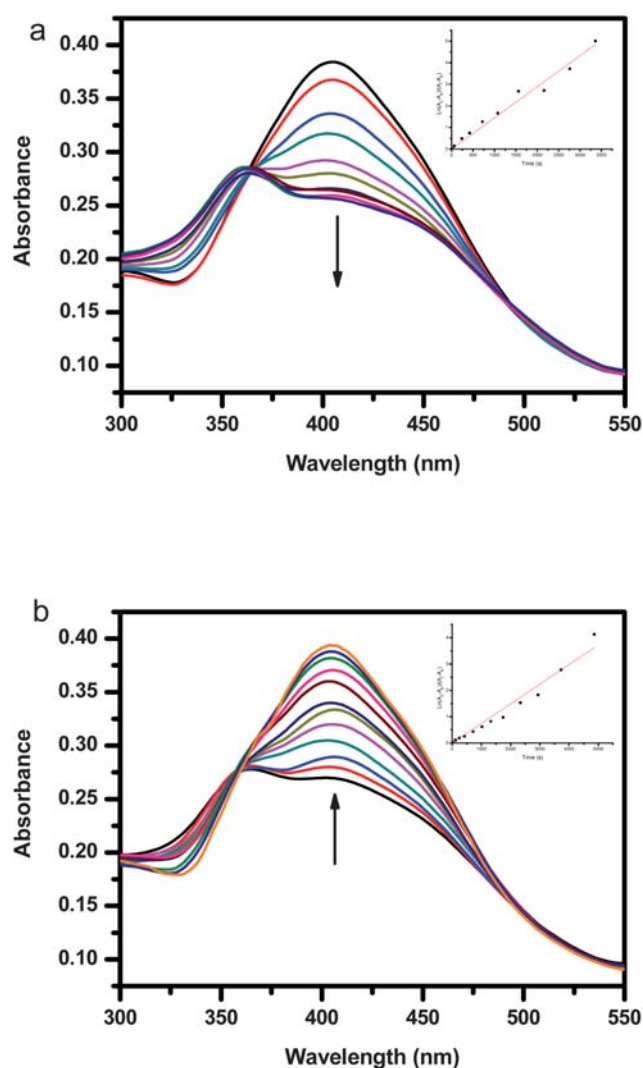


**Fig. 2** UV/Vis spectra and spectral changes of NpT5A1 suspension ( $1.2 \times 10^{-4} \text{ g mL}^{-1}$ , r.t., in DMF) upon irradiation with 405 nm light for 1, 4, 7, 12, 18, 26, 36, 46, 56, 76 min (a) and then upon irradiation with 456 nm light for 2, 4, 7, 12, 17, 22, 29, 39, 49, 62, 81, 96 min (b). Insets: first order plots for photoisomerization of the azobenzene chromophores in NpT5A1.

latter was probably caused by the inconspicuous  $\pi$ - $\pi^*$  transition due to the low proportion of AMAAB. Secondly, the rate of *trans*  $\rightarrow$  *cis* photoisomerization increased with increasing molar ratio of TRIM to AMAAB and eventually approached the value of the free AMAAB monomer (Table 1). A reasonable explanation was as follows:<sup>27</sup> a high content of TRIM in the polymer improved the porosity of the nanoparticles, which was beneficial to the sterically demanding conformational switching of the azobenzene chromophores. When the cavities within the nanomaterial were large enough, the azobenzene chromophores were able to undergo photoisomerization as if they were freely dissolved in solution. To summarize, NpT5A1 was selected for further evaluation on the basis of its overall satisfactory photo-responsive properties.

Photoisomerization of the azobenzene chromophores within the nanoparticle matrix was reversible. Fig. 3 illustrates the modulation of the absorbance of a NpT5A1 suspension upon

**Table 1** The effect of different cross-linker: monomer mole ratios on the photoisomerization kinetics of the resultant nanoparticles

	Molar ratio (TRIM:AMAAB)	Isomerization rate of <i>trans</i> → <i>cis</i> ( $\times 10^{-4} \text{ s}^{-1}$ )
NpT1A1	1 : 1	$8.40 \pm 1.1$
NpT3A1	3 : 1	$10.8 \pm 0.5$
NpT5A1	5 : 1	$14.4 \pm 0.5$
NpT10A1	10 : 1	$15.0 \pm 1.2$
NpT20A1	20 : 1	$20.3 \pm 0.7$
NpT50A1	50 : 1	$22.6 \pm 1.6$
AMAAB	$10 \mu\text{mol L}^{-1}$ DMF solution	$23.3 \pm 0.0$

alternate irradiation at 405 nm and 456 nm. The extent of reversible isomerization did not significantly decay after 11 cycles, indicating that the photo-responsive properties of NpT5A1 were stable and repeatable.

### 3.3 pH-responsive properties

The  $pK_a$  of AMAAB was measured to be  $2.15 \pm 0.06$  (see ESI<sup>†</sup>), which was consistent with the literature value.<sup>26</sup> Fig. 4a shows the UV/vis spectra of a NpT5A1 suspension at different pH. At pH = 6.86, the absorption peak at 402 nm was predominant. As the pH decreased, the 402 nm peak diminished and two new peaks at 328 and 506 nm grew dramatically. The color of the suspension changed from yellow to pink. Two isosbestic points at 360 and 475 nm were observed. Fig. 4b shows a plot of absorbance at 402 nm versus pH. Beyond pH 3, there was no significant change in the absorbance at 402 nm. However, large changes in the absorbance at 402 nm were observed when pH was in the range of 0 to 2. This is attributed to the protonation of the amino group in AMAAB into an ammonium cation. From its spectroscopic responses, the  $pK_a$  of NpT5A1 was estimated to be  $0.61 \pm 0.06$ , which was smaller than that of AMAAB. This lowering of  $pK_a$  may be due to the fact that the amino azobenzenes were embedded in a rigid environment of the polymer matrix in the nanoparticles, which prevented protons from diffusing into the polymer to reach the AMAAB, or the interior of the polymer nanoparticles is too hydrophobic for protons to diffuse freely. By switching the media

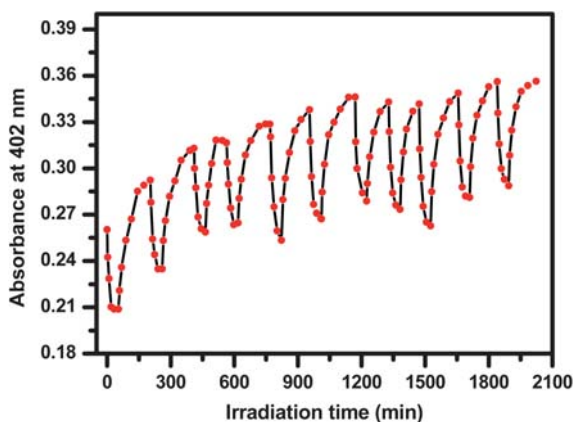


**Fig. 3** Reversibility of the photoisomerization processes of the azobenzene chromophores in the nanoparticles upon alternate irradiation at 405 nm and 456 nm respectively.

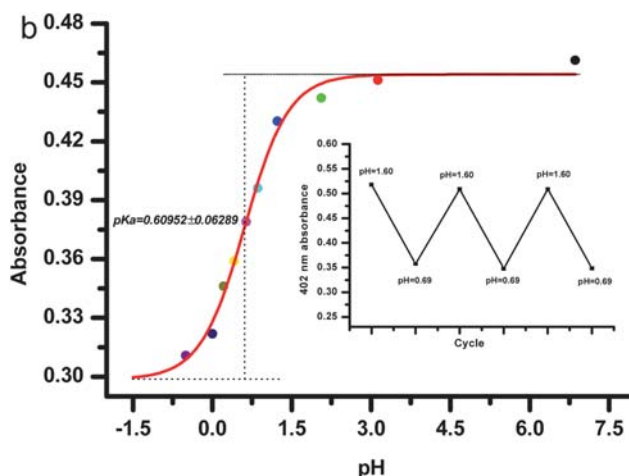
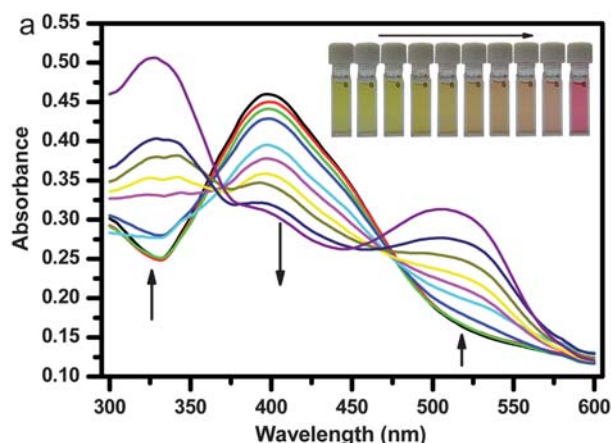


**Fig. 4** (a) UV/Vis spectra of the NpT5A1 suspension ( $0.1 \text{ mg mL}^{-1}$ , in 50% v/v ethanol-dilute HCl) at pH 6.86, 3.13, 2.06, 1.23, 0.86, 0.64, 0.41, 0.21, 0.00,  $-0.50$ . The arrow indicates the direction of decreasing pH. Inset: the color of the suspension at different pH. (b) Change in absorbance at 402 nm of NpT5A1 suspension. Inset: the plot of absorbance at 402 nm of NpT5A1 as a function of pH.

pH between 0.7 and 1.6 with  $4.0 \text{ mol L}^{-1}$  HCl and KOH solutions, the reversibility of the spectroscopic responses was demonstrated (inset of Fig. 4(b)).

### 3.4 Morphology studies

The morphology of the AMAAB-based nanoparticles was visualized by AFM. Fig. 5a and 5b show the 2D and 3D AFM images of NpT5A1, respectively. The two images show that NpT5A1 has regular spherical morphology and in the nanometre size range. As seen in Fig. 5c, the height of nanoparticles varies between 4.3 and 12.5 nm, with an average height of 7.2 nm. Fig. 5d shows the size (in diameter) distribution of the nanoparticles, 60% of the particles were of 120–280 nm, and > 85% of the particles were in the size range of 80 to 360 nm. The averaged size (in diameter) of the particles was 187 nm.

In addition, the suspension of NpT5A1 showed the Tyndall effect (Fig. 5e), which confirmed the nano-size of the particles.

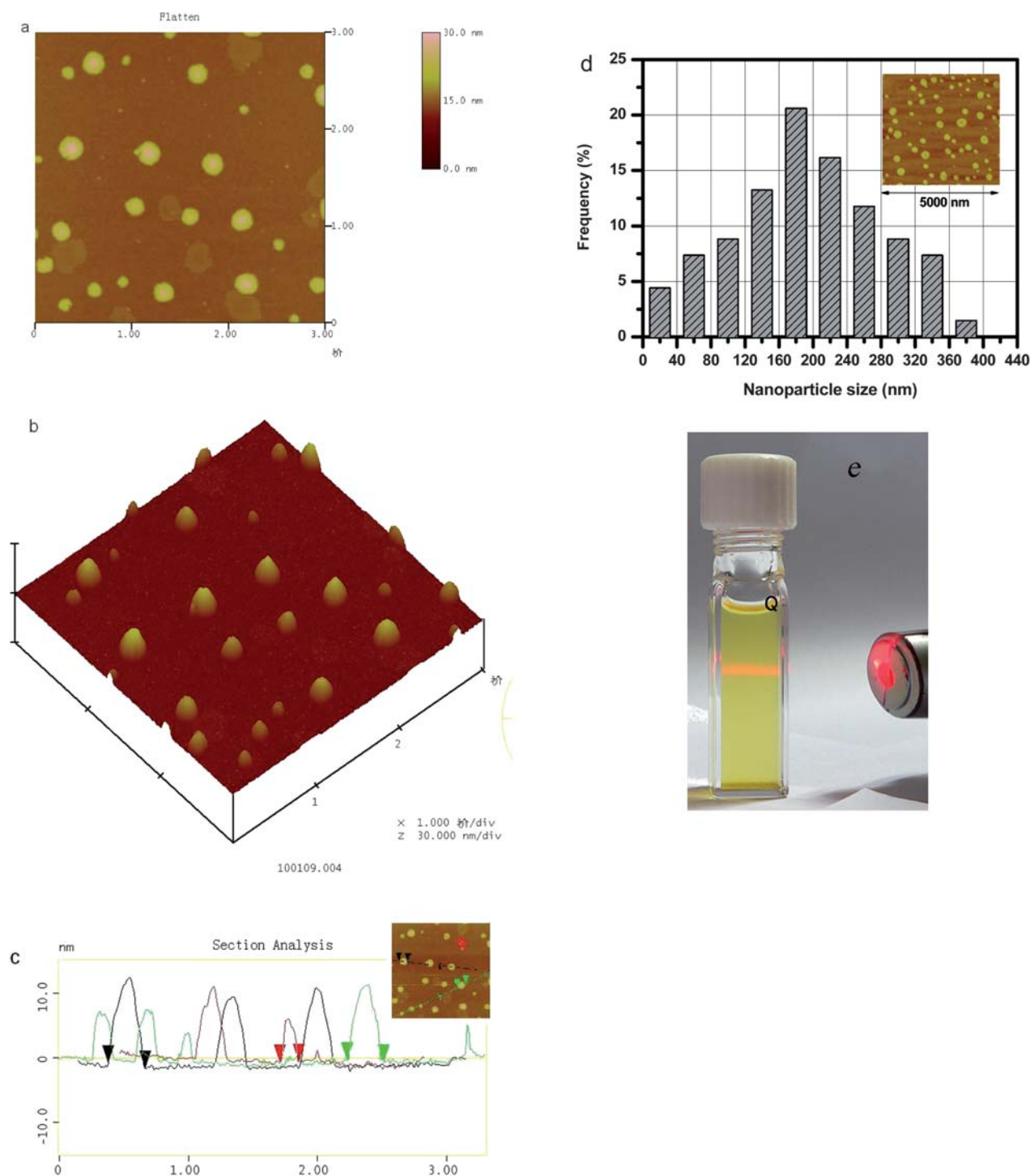


**Fig. 5** (a) A 2D-AFM image ( $3 \times 3 \mu\text{m}^2$ ) of NpT5A1 spin-coated on mica. (b) A 3D-AFM image ( $3 \times 3 \mu\text{m}^2$ ) of NpT5A1 spin-coated on mica. (c) A typical height profile of the cross section. (d) Size (diameter) distribution of NpT5A1 taken from the area of  $5 \times 5 \mu\text{m}^2$ . Inset: the AFM image ( $5 \times 5 \mu\text{m}^2$ ) of NpT5A1. The number of nanoparticles was 73. (e) A photograph of the NpT5A1 suspension ( $0.2 \text{ mg mL}^{-1}$ , in 50% v/v ethanol-water) when a light beam was irradiated from the side.

Neither the solvent (DMF) nor the AMMAB solution showed the Tyndall effect (see ESI†).

### 3.5 Thermal stability

The TG-DTG curves of NpT5A1 are shown in Fig. 6. From the TGA curve, the 5% and 50% weight loss temperatures were

around  $308 \text{ }^\circ\text{C}$  and  $373 \text{ }^\circ\text{C}$ , respectively, which indicated that NpT5A1 possessed good thermal stability. The nanoparticle exhibited a two-step weight loss process, which was within the temperature range of  $280\text{--}398 \text{ }^\circ\text{C}$  and  $398\text{--}495 \text{ }^\circ\text{C}$ , respectively. The derivative TG curves in Fig. 6 exhibited maximum weight loss rate at  $320 \text{ }^\circ\text{C}$  for the first loss range, and at  $417 \text{ }^\circ\text{C}$  for the

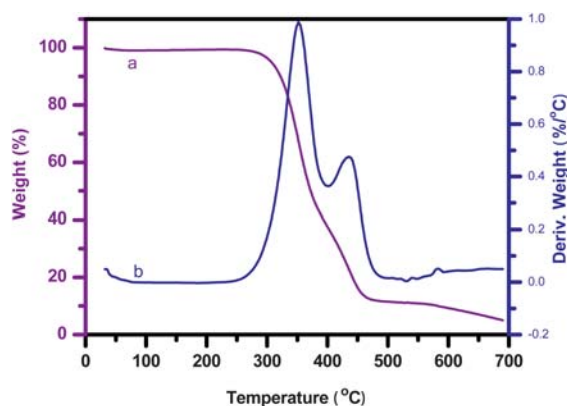


Fig. 6 TGA thermogram (curve a) and derivative of thermograms (DTG, curve b) of NpT5A1.

second, which suggested that the nanoparticles were made up of two different compositions. Near 100% weight loss occurred when temperature was above 650 °C.

#### 4. Conclusion

An amino-substituted azobenzene monomer, 4-amino-4'-methacrylatylazobenzene (AMAAB) and a series of its cross-linked polymer-based nanoparticles have been successfully synthesized and characterized. The reversible and repeatable photoisomerization of AMAAB and the AMAAB-based nanoparticles were monitored by UV/vis spectroscopy. The TRIM : AMAAB molar ratio of the nanoparticles was found to govern the kinetics of the *trans* → *cis* and *cis* → *trans* isomerization of the embedded azobenzene chromophores. NpT5A1 showed high pH sensitivity between media pH of 0 and 2. The spectroscopic transition point was observed at pH  $0.61 \pm 0.06$ . The particle size distribution of NpT5A1 was within the range of 80–360 nm with a regular spherical morphology. Thermogravimetric analysis indicated that NpT5A1 possessed good thermal stability with no obvious weight loss below 300 °C in nitrogen atmosphere. The potential applications of this kind of dual responsive nanomaterial in biotechnology, chemical sensing, pH indication and wavelength-specific photo-responding are under investigation in our laboratory.

#### Acknowledgements

The work described in this paper was supported by the National Natural Science Foundation of China (20872121), Natural Science Foundation Project of CQ CSTC (CSTC, 2009BB4001), the Fundamental Research Funds for the Central Universities (XDJK2009C011, XDJK2009C178), Research Funds for the Doctoral Program of Higher Education of China

(20090182120010), Southwest University Doctoral Fund (SWUB2008075), Postdoctoral Fund of Southwest University and the national university student innovation test plan of Southwest University (081063505).

#### Notes and references

- 1 D. Abdallah, J. Whelan, J. M. Dust, S. Hoz and E. Buncel, *J. Phys. Chem. A*, 2009, **113**, 6640–6647.
- 2 C. Alexander and K. M. Shakesheff, *Adv. Mater.*, 2006, **18**, 3321–3328.
- 3 R. Castagna, F. Vita, D. E. Lucchetta, L. Criante and F. Simoni, *Adv. Mater.*, 2009, **21**, 589–592.
- 4 C. Erben, E. P. Boden, K. L. Longley, X. L. Shi and B. L. Lawrence, *Adv. Funct. Mater.*, 2007, **17**, 2659–2666.
- 5 Z. A. Li, Q. Zeng, G. Yu, Z. Li, C. Ye, Y. Q. Liu and J. G. Qin, *Macromol. Rapid Commun.*, 2008, **29**, 136–141.
- 6 J. F. Wu, M. Q. Xu and G. C. Zhao, *Electroanalysis*, 2009, **21**, 196–200.
- 7 Z. A. Li, W. B. Wu, Q. Q. Li, G. Yu, Y. Q. LiXiaoLiu, C. Ye, J. G. Qin and Z. Li, *Angew. Chem. Int. Ed.*, 2010, **49**, 2763–2767.
- 8 Q. Q. Li, Z. Li, C. Ye and J. G. Qin, *J. Phys. Chem. B*, 2008, **112**, 4928–4933.
- 9 Q. Zeng, Z. A. Li, Z. Li, C. Ye, J. G. Qin and B. Z. Tang, *Macromolecules*, 2007, **40**, 5634–5637.
- 10 X. Q. Xue, J. Zhu, W. Zhang, Z. B. Zhang and X. L. Zhu, *Polymer*, 2009, **50**, 4512–4519.
- 11 V. Jayalakshmi, G. Hegde, G. G. Nair and S. K. Prasad, *Phys. Chem. Chem. Phys.*, 2009, **11**, 6450–6454.
- 12 A. S. Matharu, S. Jeeva and P. S. Ramanujam, *Chem. Soc. Rev.*, 2007, **36**, 1868–1880.
- 13 S. Leclair, L. Mathew, M. Giguere, S. Motallebi and Y. Zhao, *Macromolecules*, 2003, **36**, 9024–9032.
- 14 A. Pal, S. Shrivastava and J. Dey, *Chem. Commun.*, 2009, 6997–6999.
- 15 F. D. Jochum, L. zur Borg, P. J. Roth and P. Theato, *Macromolecules*, 2009, **42**, 7854–7862.
- 16 B. Luo, X. J. Song, F. Zhang, A. Xia, W. L. Yang, J. H. Hu and C. C. Wang, *Langmuir*, 2010, **26**, 1674–1679.
- 17 S. Angelos, Y. W. Yang, N. M. Khashab, J. F. Stoddart and J. I. Zink, *J. Am. Chem. Soc.*, 2009, **131**, 11344–11346.
- 18 C. B. Gong, K. L. Wong and M. H. W. Lam, *Chem. Mater.*, 2008, **20**, 1353–1358.
- 19 H. Durr and H. Bouas-Laurent, *Photochromism: molecules and systems*, Elsevier, Amsterdam, 2003.
- 20 H. K. Kim, X. S. Wang, Y. Fujita, A. Sudo, H. Nishida, M. Fujii and T. Endo, *Macromol. Chem. Phys.*, 2005, **206**, 2106–2111.
- 21 N. Delorme, J. F. Bardeau, A. Bulou and F. Poncin-Epaillard, *Langmuir*, 2005, **21**, 12278–12282.
- 22 J. H. Kim, M. Seo, Y. J. Kim and S. Y. Kim, *Langmuir*, 2009, **25**, 1761–1766.
- 23 E. J. Harbron, D. A. Vicente and M. T. Hoyt, *J. Phys. Chem. B*, 2004, **108**, 18789–18792.
- 24 L. Wu, K. Koumoto and N. Sugimoto, *Chem. Commun.*, 2009, 1915–1917.
- 25 C. B. Gong, M. H. W. Lam and H. X. Yu, *Adv. Funct. Mater.*, 2006, **16**, 1759–1767.
- 26 H. Hatanaka, K. Sugiyama, T. Nakaya and M. Imoto, *Makromolekulare Chemie-Macromolecular Chemistry and Physics*, 1974, **175**, 1855–1860.
- 27 J. Algers, P. Sperr, W. Egger, L. Liskay, G. Kogel, J. de Baerdemaeker and F. H. J. Maurer, *Macromolecules*, 2004, **37**, 8035–8042.